

# 1 **Quantifying TOLNet Ozone Lidar Accuracy during the 2014** 2 **DISCOVER-AQ and FRAPPÉ Campaigns**

3  
4 Lihua Wang<sup>1</sup>, Michael J. Newchurch<sup>1</sup>, Raul J. Alvarez II<sup>2</sup>, Timothy A. Berkoff<sup>3</sup>, Steven S.  
5 Brown<sup>2</sup>, William Carrion<sup>3,4</sup>, Russell J. De Young<sup>3</sup>, Bryan J. Johnson<sup>2</sup>, Rene Ganoé<sup>4</sup>, Guillaume  
6 Gronoff<sup>3,4</sup>, Guillaume Kirgis<sup>2,5</sup>, Shi Kuang<sup>1</sup>, Andrew O. Langford<sup>2</sup>, Thierry Leblanc<sup>6</sup>, Erin E.  
7 McDuffie<sup>2,5,7</sup>, Thomas J. McGee<sup>8</sup>, Denis Pliutau<sup>4</sup>, Christoph J. Senff<sup>2,5</sup>, John T. Sullivan<sup>8,9</sup>, Grant  
8 Sunnicht<sup>4</sup>, Laurence W. Twigg<sup>4</sup>, Andrew J. Weinheimer<sup>10</sup>

9  
10 <sup>1</sup>University of Alabama in Huntsville, Huntsville, Alabama, USA

11 <sup>2</sup>NOAA Earth System Research Laboratory, Boulder, Colorado, USA

12 <sup>3</sup>NASA Langley Research Center, Hampton, Virginia, USA

13 <sup>4</sup>Science Systems and Applications Inc., Lanham, Maryland, USA

14 <sup>5</sup>Cooperative Institute for Research in Environmental Sciences, University of Colorado, Boulder, Colorado, USA

15 <sup>6</sup>Jet Propulsion Laboratory, California Institute of Technology, Wrightwood, California, USA

16 <sup>7</sup>Department of Chemistry, University of Colorado, Boulder, Colorado, USA

17 <sup>8</sup>NASA Goddard Space Flight Center, Greenbelt, Maryland, USA

18 <sup>9</sup>Joint Center for Earth Systems Technology, Baltimore, Maryland, USA

19 <sup>10</sup>National Center for Atmospheric Research, Boulder, USA

20  
21 Correspondence to Shi Kuang (kuang@nsstc.uah.edu)

22

23 **Abstract**

24           The Tropospheric Ozone Lidar Network (TOLNet) is a unique network of lidar systems that measure high-  
25 resolution atmospheric profiles of ozone. The accurate characterization of these lidars is necessary to determine the  
26 uniformity of the network calibration. From July to August 2014, three lidars, the TROPospheric OZone (TROPOZ)  
27 lidar, the Tunable Optical Profiler for Aerosol and oZone (TOPAZ) lidar, and the Langley Mobile Ozone Lidar  
28 (LMOL), of TOLNet participated in the “Deriving Information on Surface conditions from Column and Vertically  
29 Resolved Observations Relevant to Air Quality” (DISCOVER-AQ) mission and the “Front Range Air Pollution and  
30 Photochemistry Experiment” (FRAPPÉ) to measure ozone variations from the boundary layer to the top of the  
31 troposphere. This study presents the analysis of the intercomparison between the TROPOZ, TOPAZ, and LMOL  
32 lidars, along with comparisons between the lidars and other *in situ* ozone instruments including ozonesondes and a  
33 P-3B airborne chemiluminescence sensor. The TOLNet lidars measured vertical ozone structures with an accuracy  
34 generally better than  $\pm 15\%$  within the troposphere. Larger differences occur at some individual altitudes in both the  
35 near-field and far-field range of the lidar systems, largely as expected. In terms of column average, the TOLNet  
36 lidars measured ozone with an accuracy better than  $\pm 5\%$  for both the intercomparison between the lidars and  
37 between the lidars and other instruments. These results indicate that these three TOLNet lidars are suitable for use in  
38 air quality, satellite validation, and ozone modeling efforts.

39 **1. Introduction**

40 **1.1 TOLNet**

41           The Tropospheric Ozone Lidar Network (TOLNet) provides time-height measurements of ozone from the  
42 planetary boundary layer (PBL) to the top of the troposphere at multiple locations for satellite validation, model  
43 evaluation, and scientific research (Newchurch et al., 2016; <http://www-air.larc.nasa.gov/missions/TOLNet/>).  
44 Particularly, these ozone measurements can serve to validate NASA’s first Earth Venture Instrument mission,  
45 Tropospheric Emissions: Monitoring Pollution (TEMPO), planned to launch in 2019. A second objective of TOLNet  
46 is to identify a brassboard ozone lidar instrument that would be suitable to populate a network to address an  
47 increasing need for ozone profiles by scientists and managers within the air quality, modeling, and satellite  
48 communities (Bowman, 2013).

49           TOLNet consists of five ozone lidars across the United States and one in Canada: the Table Mountain  
50 tropospheric ozone differential absorption lidar (DIAL) at NASA’s Jet Propulsion Laboratory, the Tunable Optical  
51 Profiler for Aerosol and oZone (TOPAZ) lidar at NOAA’s Earth System Research Laboratory (ESRL), the Rocket-  
52 city Ozone ( $O_3$ ) Quality Evaluation in the Troposphere (RO<sub>3</sub>QET) lidar at the University of Alabama in Huntsville  
53 (UAH), the TROPospheric OZone (TROPOZ) DIAL at NASA’s Goddard Space Flight Space Center (GSFC), the  
54 Langley Mobile Ozone Lidar (LMOL) at NASA’s Langley Research Center (LaRC), and the Autonomous Mobile  
55 Ozone Lidar Instrument for Tropospheric Experiments (AMOLITE) at Environment and Climate Change Canada.

56 All TOLNet lidars have unique configurations of original measurement design purposes, including their  
57 transmitter, receiver, and signal processing systems. Most components of these lidars are customized and differ  
58 significantly in pulse energy, repetition rate, receiver size, solar (or narrow-band) interference filter, and range  
59 resolution. These differences result in varying signal-to-noise ratios (SNRs), which impact the useful operating  
60 ranges and statistical uncertainties in ozone retrieval. The selection of the DIAL wavelengths determines the  
61 sensitivity to interference by other species, primarily aerosols. In addition, multiple lidar data processing and  
62 retrieval algorithms could also lead to different effective resolutions and lidar retrieval uncertainties (Godin et al.,  
63 1999; Leblanc et al., 2016a,b). Therefore, it is important to quantify the measurement differences between the  
64 TOLNet lidars and understand their sources before we can form a consistent TOLNet dataset. A previous  
65 intercomparison between TROPOZ and LMOL reported by Sullivan et al. (2015) concluded that the observed ozone  
66 column averages from the two lidars were within  $\pm 8\%$  of each other, and their ozone profiles were mostly within  
67  $\pm 10\%$  of each other.

## 68 **1.2 DISCOVER-AQ 2014 and FRAPPÉ Campaigns**

69 The scientific goal of the TOLNet lidars in this study was to provide continuous, high-resolution  
70 tropospheric ozone profiles to support the NASA-sponsored DISCOVER-AQ mission  
71 (<https://www.nasa.gov/larc/2014-discoveraq-campaign/>), and the National Science Foundation (NSF) and state of  
72 Colorado (CO) jointly sponsored FRAPPÉ (Dingle et al., 2016) from July to August 2014. By collaborating with  
73 FRAPPÉ, the 2014 CO study was the final stop in a series of four field campaigns by DISCOVER-AQ to understand  
74 sources, transport and chemical transformations of air pollutants, particularly those that lead to ground-level ozone  
75 formation (Crawford and Pickering, 2014).

76 Prior to the two campaigns, TOPAZ, TROPOZ, and LMOL were all deployed to the same location in Erie,  
77 CO to obtain intercomparison data at the Boulder Atmospheric Observatory (BAO) (40.050°N, 105.003°W, 1584 m  
78 above sea level, ASL). Subsequent to the BAO intercomparison, TROPOZ and LMOL re-deployed to locations near  
79 Fort Collins, CO (~60 km north-northwest of BAO) and Golden, CO (~40 km southwest of BAO), respectively, for  
80 their different scientific missions. During the DISCOVER-AQ and FRAPPÉ campaigns, balloon-borne ozonesondes  
81 were launched at selected sites. In addition, the NASA P-3B aircraft performed multiple spiral ascents and descents  
82 over several ground sites and provided measurements of ozone profiles. In this study, we compare retrievals  
83 between the three lidars and evaluate the ozone lidar accuracy using ozonesonde and P-3B aircraft measurements.  
84 These two campaigns offered a unique opportunity for the lidar validation work, as they involved so many different  
85 instruments.

## 86 **2. Instruments**

### 87 **2.1 TOLNet Lidars**

88 Table 1 lists the main hardware specifications of the three TOLNet lidars and their ozone retrieval  
89 processes, which could potentially impact the intercomparison result.

### 90 **2.1.1 TROPOZ/NASA GSFC**

91 The transmitter for TROPOZ consists of two 50-Hz Nd:YAG- lasers used to pump two Raman cells filled  
92 with Deuterium (D<sub>2</sub>) and Hydrogen (H<sub>2</sub>) gases, respectively, to generate two outgoing pulses at 289 and 299 nm.  
93 The typical pulse energies are 12 mJ at 299 nm (off-line) and 16 mJ at 289 nm (on-line) (Sullivan et al., 2014). The  
94 receiving system consists of a 45-cm-diameter Newtonian telescope for measuring far field and four smaller 2.5-cm  
95 refracting telescopes to measure near field. The 45-cm telescope has a 1-mrad field of view (FOV), and the 2.5-cm  
96 telescopes have a much wider FOV at 10 mrad. In each channel, solar interference filters with a 1-nm bandwidth  
97 decrease the amount of ambient solar light, which improves the SNR. The fundamental range resolution for the data  
98 acquisition system is 15 m (100 ns). TROPOZ measures ozone up to 16 km during daytime hours and higher  
99 altitudes at night.

### 100 **2.1.2 TOPAZ/NOAA ESRL**

101 The TOPAZ lidar is a truck-mounted scanning instrument modified from the nadir-looking airborne DIAL  
102 configuration first used in the 2006 Texas Air Quality Study (TexAQS II) (Alvarez et al., 2011; Senff et al., 2010).  
103 The lidar transmitter is based on a Ce:LiCAF laser pumped by a quadrupled Nd:YLF laser to produce three UV  
104 wavelengths, each at a 333 Hz repetition rate and tunable from 283 nm to 310 nm. The actual wavelengths used  
105 during DISCOVER-AQ 2014 were 287, 291, and 294 nm. Compared to the conventional two-wavelength DIAL, the  
106 three-wavelength configuration can potentially minimize the aerosol interference by using the dual-DIAL retrieval  
107 technique (Kovalev and Bristow, 1996) without assuming a lidar ratio and Angström exponent. However, in this  
108 study, ozone was retrieved using the 287- and 294-nm lidar signals and the standard two-wavelength DIAL  
109 algorithm because the two-wavelength retrieval was less affected by significant lidar signal noise (Alvarez et al.,  
110 2011).

111 Laser light backscattered by air molecules and aerosol particles is collected with a co-axial 50-cm diameter  
112 Newtonian telescope and then split at a 1:9 ratio into near- and far-field detection channels. The FOVs of the near-  
113 and far-field channels are controlled by different-size apertures resulting in full overlap at distances of ~300 m and  
114 ~800 m, respectively. Both channels use gated photomultipliers (PMTs) operated in analog mode with solar  
115 interference filters during the daytime. Compared to photon counting (PC) signals, the analog signal is able to  
116 maintain high linearity for strong signals and is particularly suitable for near-range measurements. The two-axis  
117 scanner on the truck sequentially points the laser beam at 2°, 6°, 20°, and 90° elevation angles in a cycle taking  
118 approximately 5 minutes. The azimuth angle was fixed throughout the experiment. The ozone profiles at these four  
119 angles are spliced together to create composite vertical profiles extending from 10 m to about 2 km AGL (Langford  
120 et al., 2016). The range resolution of the signal recording system is 6 m.

121 During the 2014 DISCOVER-AQ and FRAPPÉ campaigns, the TOPAZ ozone observations suffered from  
122 a slight, but consistent range-dependent bias created by an unknown source of noise in the data acquisition system.

123 The cause of this noise remains unknown and attempts to correct the resulting bias were unsuccessful. This bias  
124 manifests itself primarily in the low elevation angle observations ( $2^\circ$ ,  $6^\circ$ , and  $20^\circ$ ) because the signal levels and SNR  
125 are significantly lower compared to the measurements at  $90^\circ$ . For these reasons, the low angle observations below  
126 500 m were excluded from the comparisons reported within this study.

### 127 **2.1.3 LMOL/NASA LaRC**

128 The transmitter of LMOL consists of a diode-pumped Nd:YLF laser pumping a Ce:LiCAF tunable UV  
129 laser to obtain two wavelengths typically at 287.1 and 292.7 nm with a pulse energy of 0.2 mJ at 500 Hz for each  
130 wavelength. The lidar receiver system consists of a 40-cm telescope with a 1.4-mrad FOV to measure far field and  
131 another 30-cm telescope with an adjustable FOV to measure near field (De Young et al., 2017). The raw lidar  
132 signals are recorded with a 7.5-m range resolution. The LMOL data acquisition system operates in both analog and  
133 PC modes. In this study, LMOL measures ozone between 0.7 and 4.5 km. Ozone measurements for DISCOVER-AQ  
134 represent LMOL's very first remote deployment.

### 135 **2.1.4 Lidar Data Processing and Retrieval Algorithms**

136 The data processing and DIAL retrieval algorithms for the three TOLNet lidars are similar but not identical.  
137 Their details have been described by Alvarez et al. (2011), De Young et al. (2017), Langford et al. (2011), and  
138 Sullivan et al. (2015; 2014). Some basic procedures were applied on the raw lidar signals before retrievals, such as  
139 time integration (5 min for this study), dead-time correction (for PC only), background correction (subtraction),  
140 merging of PC and analog signals (for a system with both PC and analog channels), and signal-induced-bias (SIB)  
141 correction (Kuang et al., 2013). Some parameters are system dependent or empirical due to different equipment,  
142 such as the dead-time value, PC-analog timing offset, averaging range for background calculation, and SIB function  
143 form. All groups agreed to use the Brion-Daumont-Maliget (BDM) (Daumont et al., 1992; Maliget et al., 1995;  
144 Brion et al., 1993) ozone absorption cross-sections, which are temperature-dependent.

145 The ozone number density profile results from computing the derivative of the logarithm of the on-line to  
146 off-line signal ratios. Spatial (range) smoothing is usually necessary to improve the SNR and reduce the statistical  
147 errors. Various smoothing methods and their impacts on final lidar retrieval have been described by Godin et al.  
148 (1999). Both TROPOZ and LMOL groups applied a Savitzky-Golay (SG) filter with a 2<sup>nd</sup> degree polynomial on the  
149 derivative of the logarithm of the on-line to off-line signal ratios with an increasing window width to accommodate  
150 the quickly decreasing SNR. However, the SG window sizes for TROPOZ and LMOL are different due to different  
151 SNRs at each altitude. The TOPAZ group averaged lidar signal over 90 m and, then, smoothed the derivative of the  
152 logarithm of the signal ratios with a five-point least-square fit in a 450-m window. The different retrieval  
153 methodologies and parameters affect the effective vertical resolution of the retrieved ozone profiles [Leblanc et al.,  
154 2016a], as listed in Table 1. This effective resolution determines the capability of the lidars to resolve vertical ozone  
155 structure and is not equal to, but is associated with, the fitting window width.

156 All groups applied similar schemes to correct the aerosol interference. These schemes iteratively substitute  
157 derived ozone from the DIAL equation into the lidar equation to solve aerosol extinction and backscatter until both

158 aerosol and ozone converge (Alvarez et al., 2011; Kuang et al., 2011; Sullivan et al., 2014). The differential aerosol  
159 backscatter and extinction were calculated with the approximation from Browell et al. (1985). Lidars directly  
160 measure the ozone number density, and all three groups used the same temperature and pressure profiles from co-  
161 located ozonesonde measurements for Rayleigh correction, ozone mixing-ratio calculations, and computation of the  
162 temperature dependent ozone absorption cross sections.

163 Merging between different altitude channels, either different telescopes or different optical channels of the  
164 same telescope, is challenging with limited methodologies reported in the literature (Kuang et al., 2011). It is  
165 difficult to specify a method for all groups because merging is system-dependent and is affected by many factors  
166 previously described. Therefore, the three lidar groups merge the ozone profiles at different altitudes optimized for  
167 their system and SNR levels such as the example method described by Sullivan et al. (2015). As a result, additional  
168 differences between systems can occur due to the altitude channel merging.

### 169 **2.1.5 Error budget of the lidar measurements**

170 Only a brief description of the error budget of the lidar measurements is provided in this paper since the  
171 details have been discussed in the respective instrument papers (Alvarez et al., 2011; De Young et al., 2017;  
172 Sullivan et al., 2014). Table 2 presents the estimated daytime measurement uncertainties for 5 and 30-min  
173 integration time for the three lidars. Statistical uncertainties (Papayannis et al., 1990) arising from signal fluctuations  
174 are random errors and may be improved by additional averaging or smoothing. The statistical uncertainty, often  
175 referred to as measurement precision, generally increases with range due to decreasing SNR and is different for the  
176 three lidars due to their different laser power, telescope sizes, and measurement ranges. The uncertainty associated  
177 with background correction also increases with range because of decreasing signal levels. The uncertainty due to the  
178 saturation correction of the PC signals (Donovan et al., 1993) is also range dependent and typically maximizes at  
179 near range. The uncertainty arising from aerosol interference could be the largest systematic error source and can be  
180 minimized by using the appropriate correction algorithm (Eisele and Trickl, 2005; Immler, 2003; Sullivan et al.,  
181 2014). The absorption by sulfur dioxide (SO<sub>2</sub>) varies significantly with wavelength in the Hartley band. For the  
182 TOPAZ and LMOL systems, the differential SO<sub>2</sub> absorption cross section (Rufus et al., 2003) is only about 1/8 of  
183 their differential ozone absorption cross section so that the SO<sub>2</sub> interference is negligible unless very high ambient  
184 SO<sub>2</sub> concentrations are present. For TROPOZ with the 289-299-nm pair, the differential absorption cross section of  
185 SO<sub>2</sub> is about half of the ozone differential absorption cross section resulting in 1-ppb SO<sub>2</sub> being registered as 0.5-  
186 ppb ozone. Under typical atmospheric condition when SO<sub>2</sub> concentrations are less than 2 ppb (Heikes et al., 1987)  
187 and ozone concentrations are about 60 ppb, the SO<sub>2</sub>-induced error is less than 2% (Sullivan et al., 2014). However,  
188 SO<sub>2</sub> can cause a more significant ozone bias when high SO<sub>2</sub> concentrations are present such as in power plant or  
189 volcanic plumes. The estimated total lidar measurement uncertainties [Leblanc et al., 2016b] for a 30-min signal  
190 integration time are less than 20%, 12%, and 13% for TROPOZ, TOPAZ, and LMOL, respectively, within the lidar  
191 measurement ranges listed in Table 1.

## 192 2.2 Ozonesondes

193 An ozonesonde is a lightweight, balloon-borne instrument that consists of an air pump and an ozone sensor  
194 interfaced to a meteorological radiosonde. Ozonesondes are capable of measuring ozone under various weather  
195 conditions (e.g., cloudy, thunderstorm). The ozone sensor uses an electrochemical concentration cell (ECC)  
196 containing potassium iodide (KI) solution (Komhyr, 1969; Komhyr et al., 1995) to measure ozone with a precision  
197 better than  $\pm 5\%$  and an accuracy better than  $\pm 10\%$  up to 35 km altitude with a sampling interval of about 1 s and a  
198 retrieval vertical resolution of 100 m (Deshler et al., 2008; Johnson et al., 2008; Smit et al., 2007). A radiosonde  
199 attached in the same package measures air temperature, pressure, and relative humidity (Stauffer et al., 2014). The  
200 uncertainty of ozonesonde measurements is typically larger in the troposphere than that in the stratosphere (Liu et  
201 al., 2009). It has been reported that the ECC sondes suffer interference from  $\text{SO}_2$  (Flentje et al., 2010) with 1-ppb  
202  $\text{SO}_2$  being registered as -1-ppb ozone (Schenkel and Broder, 1982). Elevated  $\text{SO}_2$  can be a concern for lidar-  
203 ozonesonde intercomparison for some lidar wavelengths (e.g., 289-299 nm) because of the opposite signs of the  
204 measurement error arising from  $\text{SO}_2$  for lidar and ozonesondes. However, this is not an issue for this study since we  
205 did not find any noticeable interference from  $\text{SO}_2$  in either lidar or ozonesonde data.

## 206 2.3 Ozone Measurement Instrument onboard NASA's P-3B

207 NASA's P-3B aircraft is a pressurized, four-engine turboprop, capable of long-duration flights of 8-12  
208 hours and is based out of NASA's Wallops Flight Facility in Wallops Island, Virginia. A series of gas and aerosol  
209 instruments were outfitted within the P-3B aircraft. Ozone was measured using the National Center for Atmospheric  
210 Research (NCAR)'s 4-channel chemiluminescence instrument based on the reaction between ambient ozone and  
211 nitric oxide (NO) with an accuracy of about  $\pm 5\%$  and sampling interval of 1 s (Weinheimer et al., 1993; Ridley et  
212 al., 1992). The precision of this ozone detector is better than  $\pm 1\%$  when ambient ozone is higher than 10 ppbv. The  
213 P-3B aircraft flew spirals from 300 m to 4570 m above the surface over selected ground monitoring sites including  
214 all three lidar sites (more information in Section 3.3) during the DISCOVER-AQ 2014 campaign.

## 215 3. Results

### 216 3.1 Lidar Intercomparisons

217 The three TOLNet lidars were deployed next to the BAO tower to take simultaneous measurements before  
218 the DISCOVER-AQ/FRAPPE campaign. They were only a few hundreds of meters away from each other and were  
219 within 5 m of the same elevation (see measurement locations in Table 1).

220 Unlike stratospheric ozone lidars that focus on integrating hours of observations (Steinbrecht et al., 2009;  
221 McDermid et al., 1990), tropospheric ozone lidars need to detect ozone variations with timescales on the order of  
222 minutes, when considering ozone's shorter lifetime, smaller-scale transport, and mixing processes within the PBL  
223 and free troposphere. Therefore, we processed all lidar data on a 5-min temporal scale (signal integration time).  
224 Rayleigh correction was performed with the same atmospheric profile from the ozonesonde. Because the three lidars  
225 have different fundamental range resolutions, retrieved ozone number density values were internally interpolated on  
226 the same altitude grid with a 15-m interval for comparison.

227 Figure 1 presents the comparison of the TOPAZ and TROPOZ observed ozone at BAO from 1300 to 2135  
228 UTC (local, Mountain Daylight Time, is UTC-6) on July 11, 2014 under a partly cloudy sky condition. Data  
229 influenced by clouds were filtered out. Ozone time-height curtains from both lidars (Figure 1 a and b) show a  
230 significant (about 40%) ozone increase in the early afternoon. A total of 7655 TOPAZ and TROPOZ coincident  
231 pairs were constructed between 0.6 and 2 km AGL (altitude range over which both lidars provided valid data) over  
232 this time period. The measurement differences between the two lidars are mostly within  $\pm 5\%$  at individual grids  
233 (Figure 1 c). The value of averaged ozone concentration over some specified altitude range can represent the  
234 atmospheric ozone abundance and can be useful for satellite validation. Here, we refer to this value as ozone column  
235 average with the unit of number density, not to be confused with integrated column ozone often reported in Dobson  
236 units. The statistics of the intercomparison of the column averages is listed in Table 3. The similar  $1\sigma$  standard  
237 deviations ( $17.8$  and  $16.7 \times 10^{16} \text{ molec} \cdot \text{m}^{-3}$ ) suggest similar ozone variations captured by both lidars (also see Figure  
238 1 a and b). The mean relative difference (or normalized bias) was calculated by averaging the relative difference  
239 (i.e.,  $(\text{TROPOZ}-\text{TOPAZ})/\text{TOPAZ}$ , the denominator was arbitrarily chosen) for all paired ozone profiles. The  
240  $1.1 \pm 2.6\%$  mean relative difference suggests excellent agreement of the averaged ozone column (Figure 1 d) for 80  
241 profiles over 6.5 hours between TOPAZ and TROPOZ retrievals.

242 Figure 2 shows the TOPAZ-LMOL intercomparison for data taken on July 16, 2014 with 1902 coincident  
243 pairs from 0.9 to 2 km and between 1340 to 1730 UTC on this day. Some of the data gaps were due to low clouds  
244 blocking the lidar beams. The retrievals between the two lidars agree with each other mostly within  $\pm 10\%$  (Figure 2  
245 c). LMOL measured a mean ozone column average (Figure 2 d)  $3.8 \pm 2.9\%$  lower than TOPAZ for a total of 28  
246 paired profiles, which is significantly fewer than those from the TROPOZ-TOPAZ comparison. This small, but  
247 statistically significant ozone column difference could be due to errors in the background and saturation corrections,  
248 or biases introduced by the merging of signals or ozone retrievals from different instrument channels. Almost the  
249 same  $1\sigma$  of ozone column average in Table 3 suggests that the two lidars measured similar temporal ozone  
250 variations. The  $1-\sigma$  bars on the column average in Figure 2 (d) represent the vertical ozone variability captured by  
251 lidar at a certain time. It can be seen that the two lidars measured highly similar vertical variability as well. The  
252 consistency in capture of ozone variability for TOPA and LMOL is in part due to their similar statistical  
253 uncertainties and vertical resolutions. The generally random distribution of the relative differences in Figure 1 (c)  
254 and 2 (c) suggests overall consistent measurements with small systematic errors from all three lidars. In summary,  
255 TROPOZ, LMOL, and TOPAZ report ozone values at individual altitudes mostly within  $\pm 10\%$ , which is well within  
256 their respective uncertainties and report ozone column averages within  $\pm 3.8\%$  on average.

### 257 3.2 Lidars versus Ozonesondes

258 In order to compare the lidar data to ozonesondes, the Rayleigh- and aerosol-corrected lidar data was  
259 converted from ozone number densities to ozone mixing ratios by using sonde-measured pressure and temperature  
260 profiles, and averaged over a 30-minute interval ( $\pm 15$  minutes around sonde launch times). – Ozonesondes and  
261 lidars do not sample exactly the same atmospheric volume because the sondes typically drift horizontally. Therefore,  
262 discrepancies between the lidar and sonde observations may be in part due to real atmospheric differences. The

263 horizontal displacement of the sonde usually increases with altitude, so the distance between sonde and lidar is  
264 normally larger in the free troposphere than in the PBL. However, horizontal ozone gradients tend to be smaller in  
265 the free troposphere than in the PBL, which typically keeps atmospheric differences rather small despite the  
266 increased displacement of the sonde. The ozonesondes report values approximately every second (about every 5 m  
267 in altitude) in raw data. For comparison, the ozonesonde raw data were linearly interpolated on the lidar altitude  
268 grids with a 15-meter interval. Figure 3 shows the mean ozone mixing ratios measured by TOLNet lidars and  
269 ozonesondes, as well as their mean relative difference as function of altitude.

270 After the DISCOVER-AQ/FRAPPÉ campaign started, the TROPOZ lidar deployed to Fort Collins, CO to  
271 measure ozone. There were 11 ozonesonde profiles that were coincident and co-located with the TROPOZ  
272 measurements. The mean ozone profiles of TROPOZ and sondes (Figure 3a) show similar vertical variations with  
273 enhanced PBL and upper tropospheric ozone. The mean relative differences between TROPOZ and ozonesondes  
274 (black line in Figure 3b) are mostly within  $\pm 10\%$  up to 9 km. The local maximum of the differences at 1.8 km is  
275 associated with the merging of ozone retrievals from the near-field channel and far-field channel. The green lines in  
276 Figure 3 (b) represent the expected total measurement uncertainties including the lidar measurement uncertainties  
277 for a 30-min integration time (also see Table 2) and a 10% constant uncertainty for ozonesondes. The purple lines  
278 represent the  $1-\sigma$  standard deviations of the mean differences, which can be compared to the combined precision of  
279 lidar (i.e., statistical uncertainty) and ozonesonde (5%). The  $1-\sigma$  standard deviation increases from about 10% in the  
280 lower troposphere to about 20% in the upper troposphere as a result of increasing lidar statistical uncertainties with  
281 altitude. Below 9 km, the  $1-\sigma$  standard deviations of the mean differences are mostly located within the range of the  
282 expected uncertainties. In particular, the lidar-sonde differences around 0.5 km are significantly less than the  
283 expected uncertainties suggesting that the detection and counting systems of TROPOZ performed better than  
284 anticipated. Above 9 km, the biases increase and exceed 25% with large oscillations due to large statistical errors as  
285 a consequence of low SNR. However, ozone observations with biases between 10-20% are still representative of the  
286 upper free troposphere. On average, TROPOZ measures 2.9% higher ozone than the ozonesondes for altitudes from  
287 0.35 to 12 km. This difference can be seen as the mean difference of ozone column average between the  
288 ozonesondes and lidar for a 30-min integration time.

289 Between July 10 and July 16, a total of 10 ozonesondes were released near the BAO tower and 7 of them  
290 were coincident with TOPAZ measurements (3 on July 10, 3 on July 11, and 1 on July 16). TOPAZ mostly agrees  
291 with ozonesondes between -5% and 10% (black line in Figure 3 d). The  $1-\sigma$  standard deviation of the mean  
292 differences (purple lines) is about 5% which is close to the combined precision of TOPAZ and ozonesondes (about  
293 6%).  $1-\sigma$  of the mean differences stays almost entirely within the expected uncertainties indicative of a proper  
294 estimate of the lidar measurement uncertainties for TOPAZ in Table 2. Compared to ozonesondes, TOPAZ  
295 measures 4.4% more PBL ozone on average.

296 On July 16, there was only one pair of coincident LMOL and ozonesonde measurements at the BAO tower  
297 (Figure 3 e, f). The 30-minute averaged LMOL ozone profile agrees with the ozonesonde mostly within 0-15%  
298 between 0.95 and 4.5 km AGL with an overall average of 6.2%. The maximum bias occurring at far range (above 4

299 km) is principally due to low SNR. The bias observed at 1.5 km is likely due to the high variation in aerosol  
300 concentration and associated uncertainties in the aerosol correction. Since there is only one LMOL-ozonesonde  
301 comparison, the statistical information on the overall bias between their measurements is not available.

302 In summary, all three TOLNet lidars measured higher ozone than ozonesondes with mean ozone column  
303 differences of 2.9 % for TROPOZ, 4.4% for TOPAZ, and 6.2 % for LMOL (based on a single profile comparison).  
304 The differences between the two types of instruments and the standard deviations are mostly less than the expected  
305 uncertainties. The largest bias occurs at far-range altitudes as expected and is primarily associated with the high  
306 statistical errors arising from low SNR. The increased bias at near-range altitudes could be associated with various  
307 factors, primarily the aerosol correction and the merging of the signals or ozone retrievals from different optical or  
308 altitude channels.

### 309 **3.3 Lidars versus P-3B Chemiluminescence Instrument**

310 During the campaigns, the P-3B aircraft measured ozone profiles while doing spirals above the lidar sites.  
311 There are 34 coincident profiles between TROPOZ and the P-3B at Fort Collins, 29 between TOPAZ and the P-3B  
312 at the BAO tower, and 9 between LMOL and the P-3B at Golden, CO. The distances between the lidar and the P-3B  
313 spiral centers for these paired profiles were less than 11 km. To make coincident pairs between P-3B and lidar data,  
314 we interpolate the P-3B data onto the lidar vertical grids with a 15-m vertical resolution. Figure 4 shows the average  
315 ozone profiles measured by the lidars and the P-3B as well as their mean relative differences. TROPOZ and the P-  
316 3B agree with each other within  $\pm 5\%$  between 0.5 to 3.5 km (black lines in Figure 4, b) with a -0.8% overall average  
317 relative difference. The  $1-\sigma$  standard deviation of the mean differences (purple lines in Figure 4 b) stays almost  
318 entirely within the expected uncertainties (green lines) which include both calculated lidar measurement  
319 uncertainties and a 5% constant uncertainty for the P-3B. TOPAZ agrees with the P-3B within -11% and 3%  
320 between 0.5 and 2 km (Figure 4 c, d) with a -2.7% overall average relative difference. TOPAZ underestimates the  
321 lower-PBL (<1.5 km) ozone compared to P-3B, but when compared to ozonesondes TOPAZ overestimates ozone at  
322 many of these same altitudes (see Figure 3 d). LMOL agrees with P-3B mostly within -5% and 0% above 1800 m  
323 and within -15% and -5% between 0.7-1.8 km (Figure 4 e, f) with a -4.9% overall average relative difference. The  
324  $1-\sigma$  standard deviation of the LMOL-P3-B relative differences is mostly between 5% and 8% and is close to their  
325 combined precision (6%). The  $1-\sigma$  of the mean differences for both TOPAZ and LMOL (purple lines in Figure 4 d,  
326 f) stays within the expected uncertainty (green lines) except for the bottom altitudes.

327 In summary, TOPAZ and LMOL exhibited noticeable negative bias in the PBL compared to the P-3B while  
328 TROPOZ measured slightly lower than the P-3B. The differences between the three lidars and the P-3B are not  
329 significantly correlated suggesting that these biases were not caused by the P-3B ozone instrument. These  
330 differences could at least in part be caused by the lidar systematic errors mentioned in Section 2.1.5, but could also  
331 reflect horizontal ozone variability across the P-3B spirals, which were up to 22 km in diameter

## 332 **4. Summary and Conclusions**

333 Intercomparisons have been made between three of the six TOLNet ozone lidars (NASA GSFC's  
334 TROPOZ, NOAA ESRL's TOPAZ, and NASA LaRC's LMOL) and between the lidars and other *in situ* ozone  
335 measurement instruments using coincident data during the 2014 DISCOVER-AQ and FRAPPÉ campaigns at  
336 NOAA's BAO in Erie, CO. On average, TROPOZ, TOPAZ, and LMOL reported very similar ozone within their  
337 reported uncertainties for a 5-min signal integration time. The three lidars measured consistent ozone variations  
338 revealed in the lidar time-height curtains and in the distribution of their relative differences. From intercomparisons  
339 between the lidars and other instruments we find (1) All of the lidars measure higher ozone than ozonesondes with  
340 an average relative difference within 4.4%. The lidar profile measurements agree with the ozonesonde observations  
341 within -10-15% except at a few far-field altitudes. These results are generally consistent with Sullivan et al. (2015)  
342 from a similar ozonesonde-lidar intercomparison. (2) TROPOZ agrees with the P-3B chemiluminescence instrument  
343 below 3.5 km within  $\pm 5\%$  with a small column-averaged relative difference of -0.8%. TOPAZ and LMOL exhibit a  
344 slightly larger bias mostly between -15% and 5% below 2 km compared to the P-3B with a column-averaged  
345 difference of -2.7% and -4.9%, respectively.

346 Comparisons among the three TOLNet lidars and with *in situ* instruments suggest that the lidars are capable  
347 of capturing high-temporal tropospheric-ozone variability and of measuring tropospheric ozone with an accuracy  
348 better than  $\pm 15\%$  in terms of their vertical resolving capability and better than  $\pm 5\%$  in terms of their column  
349 measurement. These lidars have sufficient accuracy for model evaluation and satellite validation (Liu et al., 2010).  
350 Since the 2014 campaigns, all of the TOLNET lidars have been modified to improve their stability and their  
351 accuracy. The validation of these upgraded lidars will be reported in a future paper.

## 352 **Acknowledgement**

353 This work is supported by the TOLNet program developed by the National Aeronautics and Space  
354 Administration (NASA)'s Science Mission Directorate and by the National Oceanic and Atmospheric  
355 Administration Earth System Research Laboratory. Dr. John T. Sullivan's research was supported by an  
356 appointment to the NASA Postdoctoral Program at the NASA Goddard Space Flight Center, administered by  
357 Universities Space Research Association under contract with NASA. The views, opinions, and findings contained in  
358 this report are those of the authors and should not be construed as an official NOAA, NASA, or U.S. Government  
359 position, policy, or decision.

360

Table 1. Specifications for the TOLNet lidars.

	<b>TROPOZ</b>	<b>TOPAZ</b>	<b>LMOL</b>
<b>Transmitter</b>			
Laser type	Nd:YAG pumped D <sub>2</sub> , H <sub>2</sub> Raman cell	Nd:YLF pumped Ce:LiCAF	Nd:YLF pumped Ce:LiCAF
Wavelengths (nm)	288.9, 299.1	287, 291, 294	287.1, 292.7
Pulse Repetition Rate (Hz)	50	333	500
Pulse energy (mJ)	12 (299 nm), 16 (289 nm)	~0.06 for all wavelengths	0.2 for both wavelengths
<b>Detection and data acquisition system</b>			
Telescope diameter (cm)	45, 2.5	50	40, 30
FOV (mrad)	1 (45 cm), 10 (2.5 cm)	1.5 (far field channel), 3 (near field channel)	1.4 (far field channel), variable FOV (near field channel)
Signal detection type	PMT	PMT	PMT
Data acquisition type	PC	Analog	Analog and PC
Fundamental range resolution (m)	15	6	7.5
Instrument reference	(Sullivan et al., 2014)	(Alvarez et al., 2011)	(DeYoung et al., 2017)
<b>DIAL retrieval</b>			
DIAL retrieval and smoothing method	1 <sup>st</sup> -order (differential) SG filter with a 2 <sup>nd</sup> degree polynomial with an increasing window width applied on the derivative of the logarithm of the signal ratios	five-point least square fit with a 450-m window applied on the derivative of the logarithm of the signal ratios	1 <sup>st</sup> -order (differential) SG filter with a 2 <sup>nd</sup> degree polynomial, with an increasing window width applied on the derivative of the logarithm of the signal ratios
Retrieval effective resolution (m)	~100 at 1 km degrading to ~800 at 10 km	~10 below 50 m, ~30 from 50 to 150 m, ~100 from 150 to 500 m, 315 above 500 m	225 below 3 km degrading to 506 above 3 km
Aerosol correction reference	(Kuang et al., 2011; Sullivan et al., 2014)	(Alvarez et al., 2011)	(Browell et al., 1985; DeYoung et al., 2017)
Valid altitudes (km above ground level, AGL)	0.35-16	0.01-2	0.7-4.5
<b>Measurement location</b>			
Latitude (°N)	40.050	40.045	40.050
Longitude (°W)	105.000	105.006	105.004
Elevation (m ASL)	1584	1587	1584

364 **Table 2. Maximum 1- $\sigma$  uncertainties for TROPOZ, TOPAZ and LMOL daytime ozone measurements within their**  
 365 **measurable range for the 5 and 30-min integration time.**

Source	Maximum uncertainty within each lidar's measurement range					
	5-min integration			30-min integration		
Lidar	TROPOZ	TOPAZ	LMOL	TROPOZ	TOPAZ	LMOL
Measurement range (km)	0.35-16	0.01-2	0.7-4.5	0.35-16	0.01-2	0.7-4.5
Statistical Uncertainty <sup>a</sup>	20%	8%	15%	8%	3%	6%
Background correction <sup>a</sup>	10%	3%	5%	10%	3%	5%
Saturation correction <sup>b</sup>	1%	N/A	5%	1%	N/A	5%
Aerosol interference	10%	10%	10%	10%	10%	10%
Interference by SO <sub>2</sub> , NO <sub>2</sub> , O <sub>2</sub> dimer	3%	1%	1%	3%	1%	1%
Differential Rayleigh scattering	3%	3%	3%	3%	3%	3%
Ozone absorption cross section	3%	3%	3%	3%	3%	3%
Total uncertainty <sup>c</sup>	25%	14%	19%	20%	12%	13%

366 <sup>a</sup> Range dependent and increasing with altitude.

367 <sup>b</sup> Range dependent and typically maximized at the near range.

368 <sup>c</sup> Total root-mean-square uncertainty by considering the range dependent uncertainties (also see Figure 3 and 4).

369

370

371

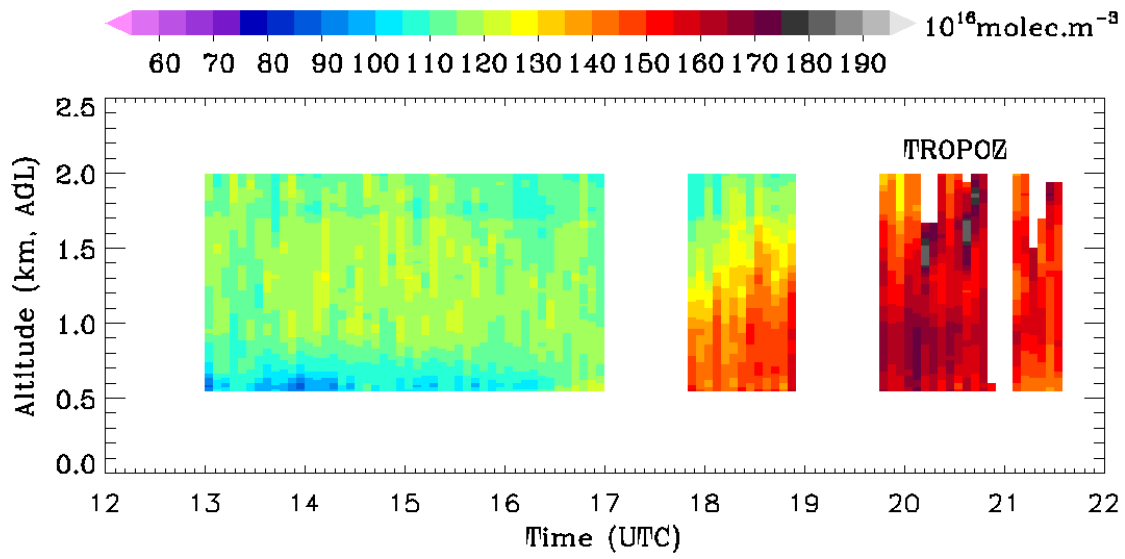
372

**Table 3. Comparisons of the ozone column average measured by TROPOZ, TOPAZ, and LMOL.**

Date	UTC time range	Altitude range (km)	Lidar	Number of the paired profiles	Mean ozone column average (10 <sup>16</sup> molec·m <sup>-3</sup> )	1 $\sigma$ of the ozone column average (10 <sup>16</sup> molec·m <sup>-3</sup> )	Mean relative difference*	1 $\sigma$ of the difference
7/11/2014	1300-2135	0.6-2	TROPOZ/TOPAZ	80	127.3/128.6	17.8/16.7	-1.1%	2.6%
7/16/2014	1335-1730	0.9-2	LMOL/TOPAZ	28	98.1/102.0	13.1/13.0	-3.8%	2.9%

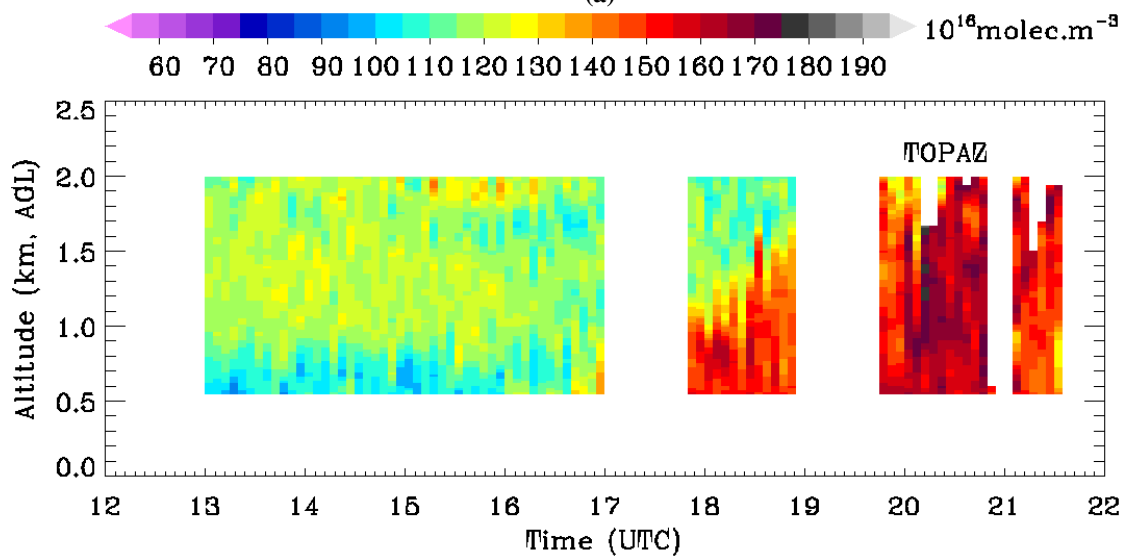
373 \* Equal to mean (A-B)/B for A/B in 'Lidar' column for all paired profiles.

374



375  
376

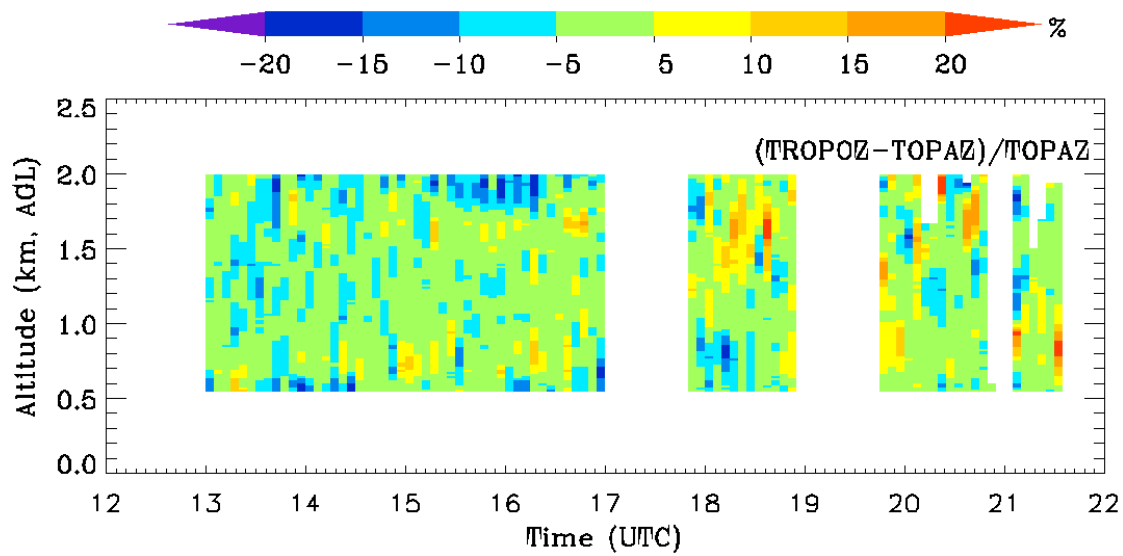
(a)



377  
378

(b)

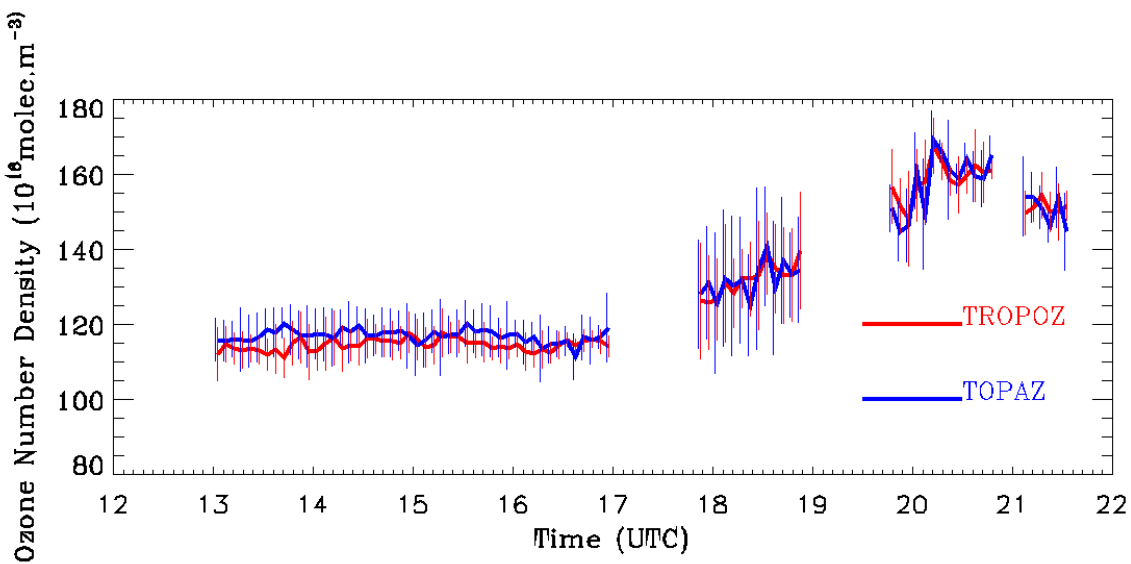
379



380

381

(c)



382

383

(d)

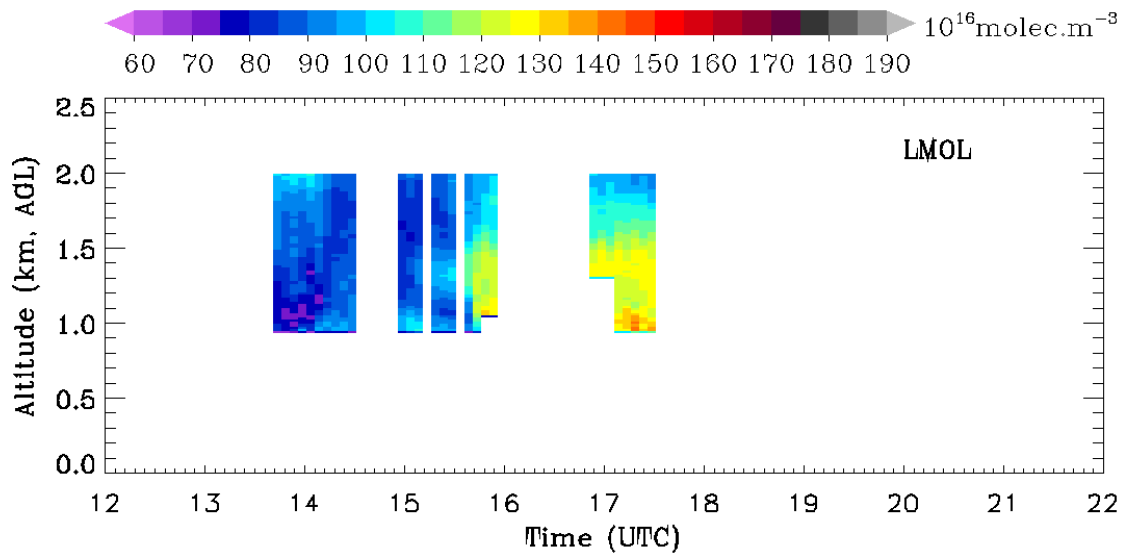
384 Figure 1. Comparisons of ozone measured by TROPOZ and TOPAZ. (a) Ozone number densities measured by TROPOZ.

385 (b) Ozone number densities measured by TOPAZ. (c) Their relative percent differences,  $(\text{TROPOZ} - \text{TOPAZ}) / \text{TOPAZ}$ . (d)

386 Column averages measured by the TROPOZ and TOPAZ as well as their  $1-\sigma$  standard deviations. TROPOZ measures

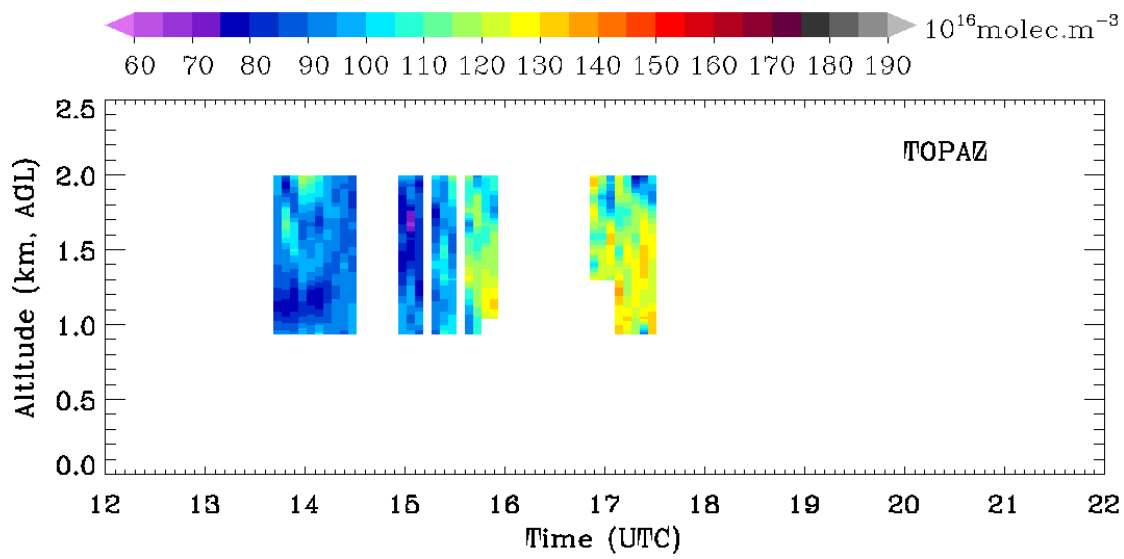
387  $1.1 \pm 2.6\%$  lower ozone column average than TOPAZ.

388



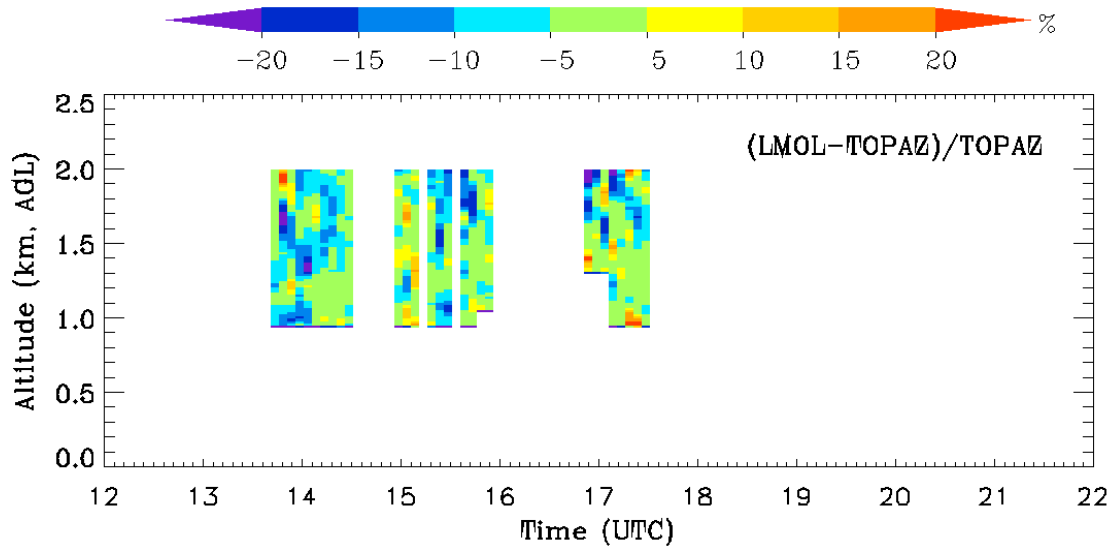
389  
390

(a)



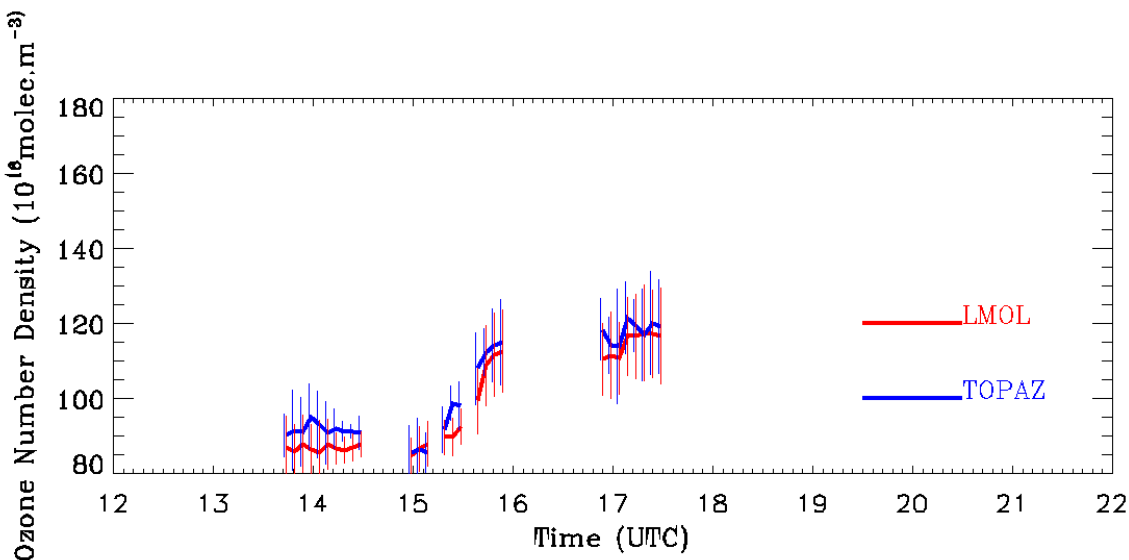
391  
392

(b)



393  
394

(c)

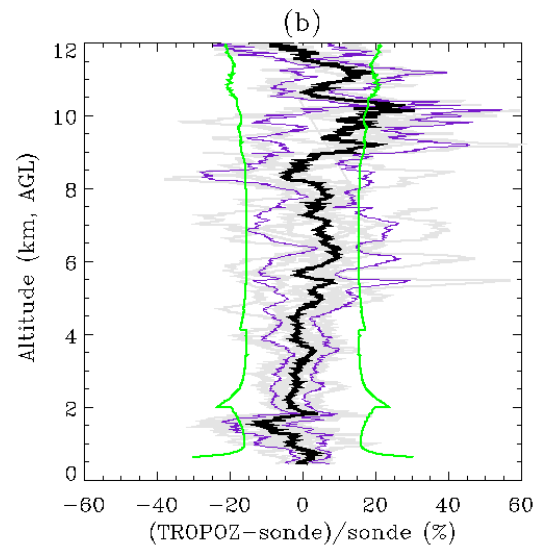
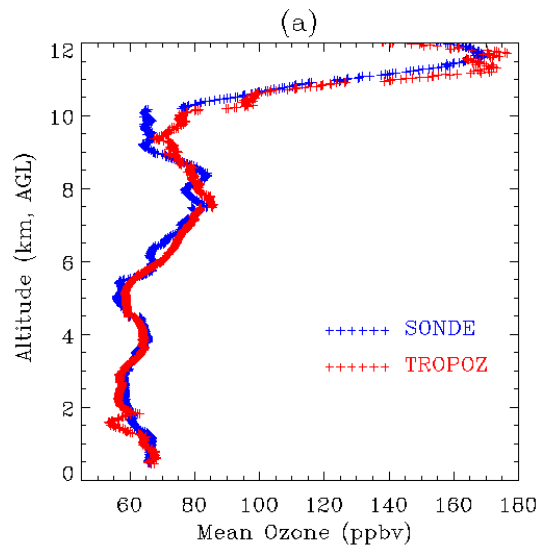


395  
396

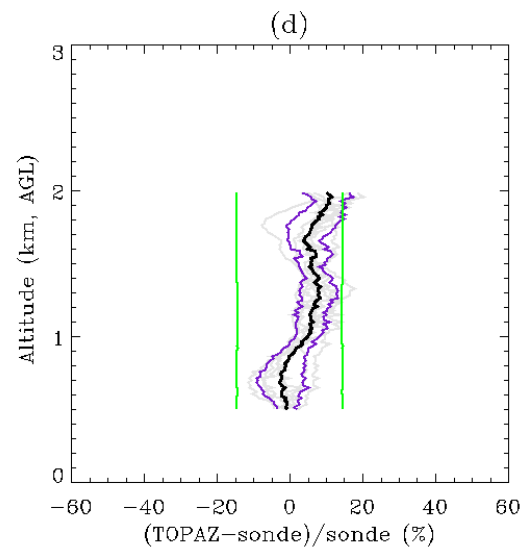
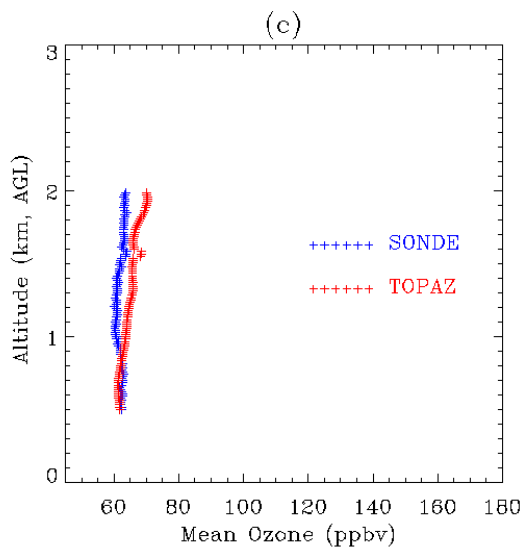
(d)

397 **Figure 2. Comparisons of ozone measured by LMOL and TOPAZ. (a) LMOL-measured ozone number densities. (b)**  
 398 **TOPAZ-measured ozone number densities. (c) Their relative percent differences,  $(LMOL-TOPAZ)/TOPAZ$ . (d) Column**  
 399 **averages measured by LMOL and TOPAZ as well as their  $1-\sigma$  standard deviations. LMOL measures  $3.8 \pm 2.9\%$  lower**  
 400 **ozone column average than TOPAZ.**

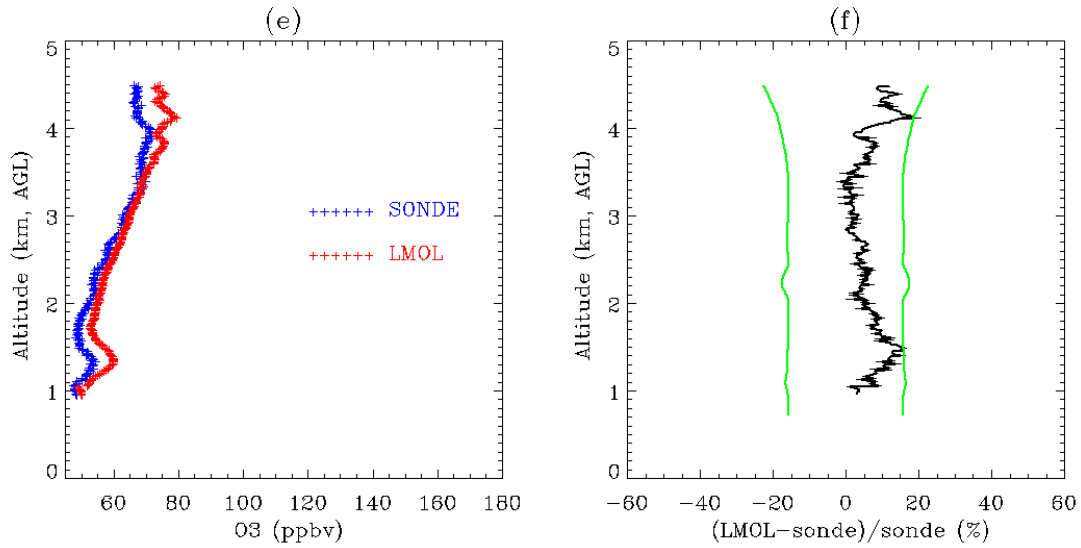
401



402



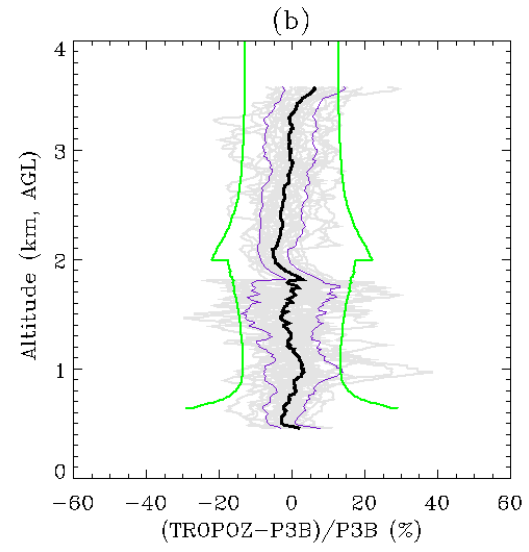
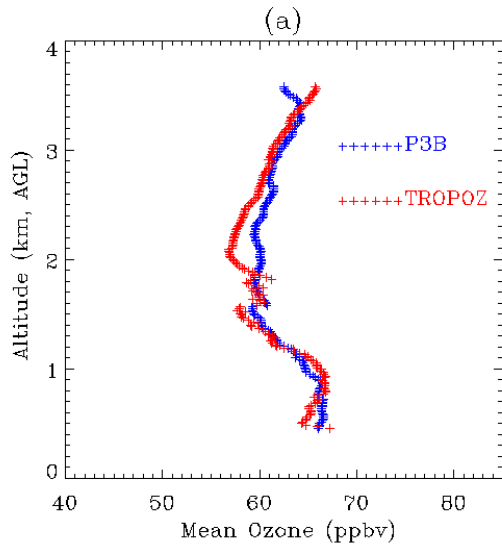
403



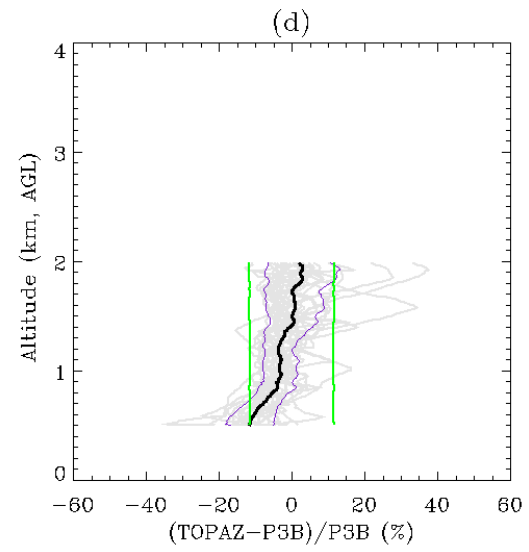
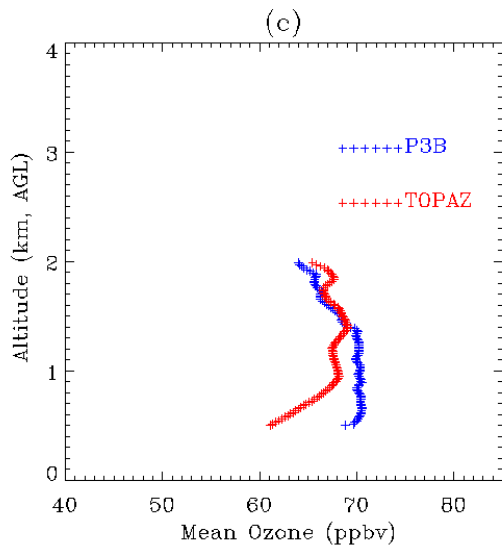
404

405 **Figure 3. Comparisons of lidar and ozonesonde measurements. (a) Average ozone profiles measured by TROPOZ and**  
 406 **ozonesondes at Fort Collins, CO (11 pairs). (b) Mean relative difference (black) between TROPOZ and ozonesondes as**  
 407 **well as the 1- $\sigma$  standard deviations (purple). (c) Average ozone profiles measured by TOPAZ and ozonesondes at BAO**  
 408 **Tower (7 pairs). (d) Mean relative difference (black) between TOPAZ and ozonesondes as well as the 1- $\sigma$  standard**  
 409 **deviations (purple). (e) Average ozone profiles measured by LMOL and ozonesonde at the BAO tower (1 pair). (f)**  
 410 **Relative difference between LMOL and ozonesonde. The gray lines represent the individual difference profiles between**  
 411 **the lidar and sondes. The green lines represent the expected uncertainties including the 30-min lidar measurement**  
 412 **uncertainties (also see Table 2) and a 10% constant uncertainty for ozonesondes.**

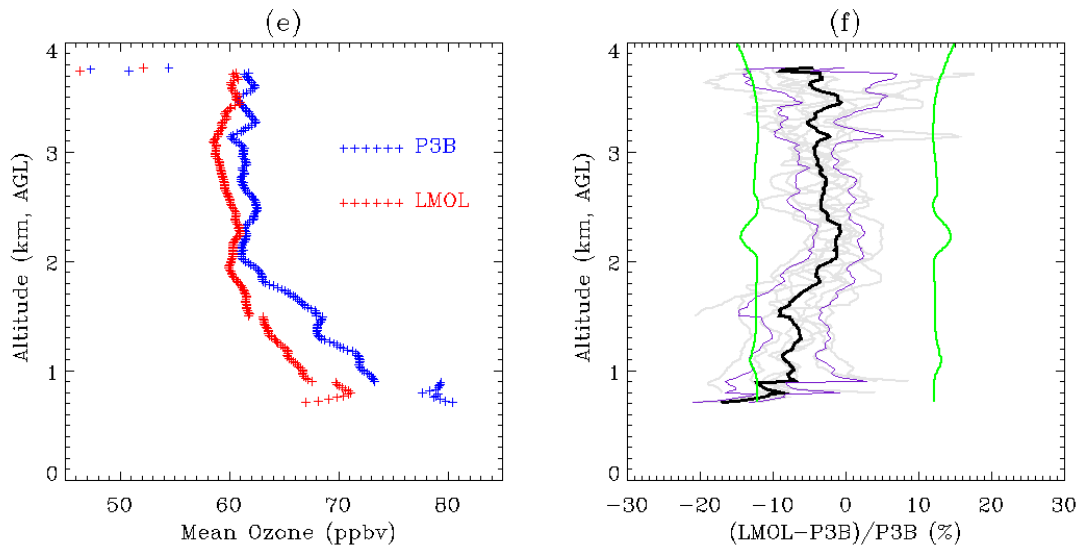
413



414



415



416  
417

418 **Figure 4. Intercomparison between the lidar and P-3B measurements. (a) Average ozone profiles measured by TROPOZ**  
 419 **and P-3B at Fort Collins, CO (34 profiles). (b) Mean relative difference (black) between TROPOZ and P-3B data as well**  
 420 **as the 1- $\sigma$  standard deviation (purple). (c) Average ozone profiles measured by TOPAZ and P-3B at the BAO Tower (29**  
 421 **profiles). (d) Mean relative difference between TOPAZ and P-3B data as well as the 1- $\sigma$  standard deviation (purple). (e)**  
 422 **Average ozone profiles measured by LMOL and P-3B at Golden, CO (9 profiles). (f) Mean relative difference between**  
 423 **LMOL and P-3B data as well as the 1- $\sigma$  standard deviation (purple). The gray lines represent the individual difference**  
 424 **profiles between the lidar and sondes. The green lines represent the expected uncertainties including the 30-min lidar**  
 425 **measurement uncertainties (also see Table 2) and a 10% constant uncertainty for ozonesondes.**

426  
427

## References

- 428  
429  
430 Alvarez, R. J., Senff, C. J., Langford, A. O., Weickmann, A. M., Law, D. C., Machol, J. L., Merritt, D. A.,  
 431 Marchbanks, R. D., Sandberg, S. P., Brewer, W. A., Hardesty, R. M., and Banta, R. M.: Development and  
 432 Application of a Compact, Tunable, Solid-State Airborne Ozone Lidar System for Boundary Layer  
 433 Profiling, *J. Atmos. Oceanic Tech.*, 28, 1258-1272, 10.1175/JTECH-D-10-05044.1, 2011.  
 434 Bowman, K. W.:  
 435 Toward the next generation of air quality monitoring: Ozone. *Atmos. Environ.*, 80, 571-583, 2013.  
 436 Brion, J., Chakir, A., Daumont, D., and Malicet, J.: High-resolution laboratory absorption cross section of O<sub>3</sub>  
 437 temperature effect, *Chem. Phys. Lett.*, 213, 510-512, 1993.  
 438 Browell, E. V., Ismail, S., and Shipley, S. T.: Ultraviolet DIAL measurements of O<sub>3</sub> profiles in regions of spatially  
 439 inhomogeneous aerosols, *Appl. Opt.*, 24, 2827-2836, 1985.  
 440 Crawford, J. H., and Pickering, K. E.: DISCOVER-AQ: Advancing strategies for air quality observations in the next  
 441 decade, *Environ. Manage.*, 4-7, 2014.  
 442 Daumont, D., Brion, J., Charbonnier, J., and Malicet, J.: Ozone UV spectroscopy I: Absorption cross-sections at  
 443 room temperature, *J. Atmos. Chem.*, 15, 145-155, 1992.  
 444 De Young, R., Carrion, W., Ganoe, R., Pliutau, D., Gronoff, G., Berkoff, T., and Kuang, S.: Langley mobile ozone  
 445 lidar: ozone and aerosol atmospheric profiling for air quality research, *Appl. Opt.*, 56, 721,  
 10.1364/ao.56.000721, 2017.

446 Deshler, T., Mercer, J. L., Smit, H. G. J., Stubi, R., Levrat, G., Johnson, B. J., Oltmans, S. J., Kivi, R., Thompson,  
447 A. M., Witte, J., Davies, J., Schmidlin, F. J., Brothers, G., and Sasaki, T.: Atmospheric comparison of  
448 electrochemical cell ozonesondes from different manufacturers, and with different cathode solution  
449 strengths: The balloon experiment on standards for ozonesondes., *J. Geophys. Res.*, 113, D04307, doi:  
450 10.1029/2007/JD008975, 2008.

451 Dingle, J. H., Vu, K., Bahreini, R., Apel, E. C., Campos, T. L., Flocke, F., Fried, A., Herndon, S., Hills, A. J.,  
452 Hornbrook, R. S., Huey, G., Kaser, L., Montzka, D. D., Nowak, J. B., Reeves, M., Richter, D., Roscioli, J.  
453 R., Shertz, S., Stell, M., Tanner, D., Tyndall, G., Walega, J., Weibring, P., and Weinheimer, A.: Aerosol  
454 optical extinction during the Front Range Air Pollution and Photochemistry Experiment (FRAPPÉ) 2014  
455 summertime field campaign, Colorado, USA, *Atmos. Chem. Phys.*, 16, 207-217, doi:10.5194/acp-16-  
456 11207-2016, 2016.

457 Donovan, D. P., Whiteway, J. A. and Carswell, A. I.: Correction for nonlinear photon-counting effects in lidar  
458 systems, *Appl. Opt.*, 32, 6742-6753, 1993.

459 Eisele, H., and Trickl, T.: Improvements of aerosol algorithm in ozone lidar data processing by use of evolutionary  
460 strategies, *Appl. Opt.*, 44, 2638-2651, 2005.

461 Flentje, H., Claude, H., Elste, T., Gilge, S., Köhler, U., Plass-Dülmer, C., Steinbrecht, W., Thomas, W., Werner, A.  
462 and Fricke, W.: The Eyjafjallajökull eruption in April 2010—detection of volcanic plume using in-situ  
463 measurements, ozone sondes and lidar-ceilometer profiles, *Atmos. Chem. Phys.* 10, 10085-10092, 2010.

464 Godin, S. M., Carswell, A. I., Donovan, D. P., Claude, H., Steinbrecht, W., McDermid, I. S., McGee, T. J., Gross,  
465 M. R., Nakane, H., Swart, D. P. J., Bergwerff, H. B., Uchino, O., Gathen, P. v. d., and Neuber, R.: Ozone  
466 differential absorption lidar algorithm intercomparison, *Appl. Opt.*, 38, 6225-6236, 1999.

467 Heikes, B.G., Kok, G.L., Walega, J.G. and Lazrus, A.L.: H<sub>2</sub>O<sub>2</sub>, O<sub>3</sub> and SO<sub>2</sub> measurements in the lower troposphere  
468 over the eastern United States during fall, *J. Geophys. Res.: Atmospheres*, 92, 915-931, 1987.

469 Immler, F.: A new algorithm for simultaneous ozone and aerosol retrieval from tropospheric DIAL measurements,  
470 *Appl. Phys. B*, 76, 593-596, 2003.

471 Johnson, B. J., Helmig, D., and Oltmans, S.: Evaluation of ozone measurements from a tethered balloon-sampling  
472 platform at South Pole Station in December 2003, *Atmos. Environ.*, 42, 2780-2878,  
473 10.1016/j.atmosenv.2007.03.043, 2008.

474 Komhyr, W. D.: Electrochemical cells for gas analysis, *Ann. Geophys.*, 25, 203-210, 1969.

475 Komhyr, W. D., Barnes, R. A., Brothers, G. B., Lanthrop, J. A., and Opperman, D. P.: Electrochemical  
476 concentration cell ozonesonde performance evaluation during STOIC 1989, *J. Geophys. Res.*, 100, 9231-  
477 9244, 1995.

478 Kovalev, V. A., and Bristow, M. P.: Compensational three-wavelength differential-absorption lidar technique for  
479 reducing the influence of differential scattering on ozone-concentration measurements, *Appl. Opt.*, 35,  
480 4790-4797, 1996.

481 Kuang, S., Burris, J. F., Newchurch, M. J., Johnson, S., and Long, S.: Differential Absorption Lidar to Measure  
482 Subhourly Variation of Tropospheric Ozone Profiles, *IEEE Transactions on Geoscience and Remote  
483 Sensing*, 49, 557-571, 10.1109/TGRS.2010.2054834, 2011.

484 Kuang, S., Newchurch, M. J., Burris, J., and Liu, X.: Ground-based lidar for atmospheric boundary layer ozone  
485 measurements, *Appl. Opt.*, 52, 3557-3566, 10.1364/AO.52.003557, 2013.

486 Langford, A. O., Senff, C. J., Alvarez II, R. J., banta, R. M., Hardesty, M., Parrish, D. D., and Ryerson, T. B.:  
487 Comparison between the TOPAZ airborne ozone lidar and in situ measurements during TexAQS 2006, *J.  
488 Atmos. Oceanic Technol.*, 28, 1243-1257, doi: <http://dx.doi.org/10.1175/JTECH-D-10-05043.1> 2011.

489 Langford, A. O., Alvarez, R. J., Brioude, J., Fine, R., Gustin, M., Lin, M. Y., Marchbanks, R. D., Pierce, R. B.,  
490 Sandberg, S. P., Senff, C. J., Weickmann, A. M., and Williams, E. J.: Entrainment of stratospheric air and  
491 Asian pollution by the convective boundary layer in the Southwestern U.S, *Journal of Geophysical  
492 Research: Atmospheres*, n/a-n/a, 10.1002/2016JD025987, 2016.

493 Leblanc, T., Sica, R. J., van Gijsel, J. A. E., Godin-Beekmann, S., Haefele, A., Trickl, T., Payen, G., and Gabarrot,  
494 F.: Proposed standardized definitions for vertical resolution and uncertainty in the NDACC lidar ozone and  
495 temperature algorithms – Part 1: Vertical resolution, *Atmos. Meas. Tech.*, 9, 4029-4049, 10.5194/amt-9-  
496 4029-2016, 2016a.

497 Leblanc, T., Sica, R.J., Van Gijsel, J.A., Godin-Beekmann, S., Haefele, A., Trickl, T., Payen, G. and Liberti, G.,  
498 2016. Proposed standardized definitions for vertical resolution and uncertainty in the NDACC lidar ozone  
499 and temperature algorithms—Part 2: Ozone DIAL uncertainty budget. *Atmospheric Measurement  
500 Techniques*, 9(8), pp.4051-4078, 2016b.

501 Liu, G., Tarasick, D. W., Fioletov, V. E., Sioris, C. E. and Rochon, Y. J.: Ozone correlation lengths and  
502 measurement uncertainties from analysis of historical ozonesonde data in North America and Europe. *J. of*  
503 *Geophys. Res.*, 114, D04112, 2009.

504 Liu, X., Bhartia, P. K., Chance, K., Spurr, R. J. D., and Kurosu, T. P.: Ozone profile retrievals from the Ozone  
505 Monitoring Instrument, *Atmos. Chem. Phys.*, 10, 2521-2537, 2010.

506 Malicet, C., Daumont, D., Charbonnier, J., Parisse, C., Chakir, A., and Brion, J.: Ozone UV spectroscopy. II.  
507 Absorption cross-sections and temperature dependence, *J. Atmos. Chem.*, 21, 263-273, 1995.

508 McDermid, I. S., Godin, S. M., Lindqvist, L. O., Walsh, T. D., Burris, J., Butler, J., Ferrare, R., Whiteman, D., and  
509 McGee, T. J.: Measurement intercomparison of the JPL and GSFC stratospheric ozone lidar systems, *Appl.*  
510 *Opt.*, 29, 4671-4676, 1990.

511 Newchurch, M. J., Kuang, S., Leblanc, T., Alvarez, R. J., Langford, A. O., Senff, C. J., Burris, J. F., McGee, T. J.,  
512 Sullivan, J. T., DeYoung, R. J., and Al-Saadi, J.: TOLNET - A Tropospheric Ozone Lidar Profiling  
513 Network for Satellite Continuity and Process Studies, The 27th International Laser Radar Conference  
514 (ILRC 27), 2016,

515 Papayannis, A., Ancellet, G., Pelon, J., and Mégie, G.: Multiwavelength lidar for ozone measurements in the  
516 troposphere and the lower stratosphere, *Appl. Opt.*, 29, 467-476, 1990.

517 Ridley, B. A., Grahek, F. E., and Walega, J. G.: A small high-sensitivity, medium-response ozone detector suitable  
518 for measurements from light aircraft, *J. Atmos. Oceanic Tech.*, 9, 142-148, 1992.

519 Rufus, J., Stark, G., Smith, P.L., Pickering, J.C. and Thorne, A.P.: High - resolution photoabsorption cross section  
520 measurements of SO<sub>2</sub>, 2: 220 to 325 nm at 295 K, *J. Geophys. Res.: Planets*, 108, 2003

521 Schenkel, A., and Broder, B.: Interference of some trace gases with ozone measurements by the KI method, *Atmos.*  
522 *Environ.* 16, 2187-2190, 1982.

523 Senff, C. J., Alvarez, R. J., Hardesty, R. M., Banta, R. M., and Langford, A. O.: Airborne lidar measurements of  
524 ozone flux downwind of Houston and Dallas, *J. Geophys. Res.: Atmospheres*, 115, D20,  
525 10.1029/2009JD013689, 2010.

526 Smit, H. G. J., Straeter, W., Johnson, B. J., Oltmans, S. J., Davies, J., Tarasick, D. W., Hoegger, B., Stubi, R.,  
527 Schmidlin, F. J., Northam, T., Thompson, A. M., Witte, J. C., Boyd, I., and Posny, F.: Assessment of the  
528 performance of ECC-ozonesondes under quasi-flight conditions in the environmental simulation chamber:  
529 Insights from the Juelich Ozone Sonde Intercomparison Experiment (JOSIE), *J. Geophys. Res.*, 112,  
530 D19306, doi:10.1029/2006JD007308, 2007.

531 Stauffer, R. M., Morris, G. A., Thompson, A. M., Joseph, E., Coetzee, G. J. and Nalli, N. R.: Propagation of  
532 radiosonde pressure sensor errors to ozonesonde measurements, *Atmos. Meas. Tech.*, 7, 65-79, 2014.

533 Steinbrecht, W., McGee, T. J., Twigg, L. W., Claude, H., Schönnenborn, F., Sumnicht, G. K., and Silbert, D.:  
534 Intercomparison of stratospheric ozone and temperature profiles during the October 2005 Hohenpeißenberg  
535 Ozone Profiling Experiment (HOPE), *Atmos. Meas. Tech.*, 2, 125-145, 2009.

536 Sullivan, J. T., McGee, T. J., Sumnicht, G. K., Twigg, L. W., and Hoff, R. M.: A mobile differential absorption lidar  
537 to measure sub-hourly fluctuation of tropospheric ozone profiles in the Baltimore-Washington, D.C. region,  
538 *Atmos. Meas. Tech.*, 7, 3529-3548, 10.5194/amt-7-3529-2014, 2014.

539 Sullivan, J. T., McGee, T. J., DeYoung, R., Twigg, L. W., Sumnicht, G. K., Pliutau, D., Knepp, T., and Carrion, W.:  
540 Results from the NASA GSFC and LaRC Ozone Lidar Intercomparison: New Mobile Tools for  
541 Atmospheric Research, *J. Atmos. Oceanic Tech.*, 32, 1779-1795, doi:10.1175/JTECH-D-14-00193.1, 2015.

542 Weinheimer, A. J., Walega, J. G., Ridley, B. A., Satche, G. W., Anderson, B. E., and Collins Jr., J. E.: Stratospheric  
543 NO<sub>y</sub> measurements on the NASA DC-8 during AASE II, *Geophys. Res. Lett.*, 20, 2563-2566, 1993.

544